DESIGN AND ANALYSIS OF A LIGHT CARGO UAV PROTOTYPE

[1]Anastasios P. Kovanis[*], [2]Vangelis Skaperdas, [3]John A. Ekaterinaris
[1]Graduate Student, Mechanical Engineering & Aeronautics Department, School of Engineering, University of Patras, 26500, Patras, Greece
[2]Engineer, BETA CAE Systems S.A., Thessaloniki, Greece
[3]Professor, Mechanical Engineering & Aeronautics Department, School of Engineering, University of Patras, 26500, Patras, and FORTH/IACM, Greece, Associate Fellow AIAA

KEYWORDS - UAV, aerodynamics, design, cfd, analysis

ABSTRACT - A light cargo unmanned air vehicle (UAV) was designed, constructed, and tested in flight. This UAV was designed and build according to the specifications of the Air Cargo Challenge 2009 Design, Build & Fly European student competition. The basic aerodynamic and stability analysis that was used in the preliminary phase of the light UAV design are presented. Flight stability analysis was based on the linearized theory. The preliminary aerodynamic analysis was based on Navier-Stokes solutions for wing and wing-body configurations. The conceptual design was constructed and successfully tested. Further aerodynamic analysis for the full configuration was carried out to evaluate the performance during the flight envelope. The findings of this analysis could be utilized to further improve the aerodynamics of the existing design, and enhance stability and performance characteristics of the light cargo UAV.

TECHNICAL PAPER

1. INTRODUCTION

The technology of large and small unmanned air vehicles (UAV's) is rapidly emerging in the European countries and the US. Te design principles for UAV's are similar to the principles developed over the years and used successfully for the design of commercial and general purpose aircraft. The size of UAV varies according to the purpose of their utility. In many cases the design and constructions of UAV's faces new challenges and, as a result of these new requirements, several recent works[1-10] are concerned with the design of innovative UAV's. Initial thrust for improved UAV designs was given due to their importance in military operations. However, nowadays there is increased interest for UAV applications in the public sector for a vast area of applications[11-13] ranging from rescue operations to surveillance and monitoring.
The first UAV designs that appeared in the early nineties were based on the general design principles for full aircraft and findings of experimental inverstigations[14]. Often the main limitation of commercial general purpose UAV's is low cost. An important area of UAV technology is the design of autonomous navigation systems, however, this subject is outside the scope of this work. The tremendous increase of computing power in the last two decades and developments of general purpose reliable CFD software packages made possible the use of full configuration CFD techniques for the design, evaluation, and optimization of modern UAV. Several recent works[14-16] used CFD analysis for new UAV designs even for cases where innovative unconventional designs were employed.
The competition Air Cargo Challenge was initiated by APAE (Portuguese Association of Aeronautics & Space) in 2003, inspired by the North American Design Build & Fly (DBF) aircraft university competitions. The 2009 edition of the competition was organized by AeroUBI EUROAVIA Covilha (Association of Aeronautical Engineering of University of Beira Interior) in 28 - 30 August 2009 at Covilha, Portugal. The objective of the teams participated was to design, document, build and fly a radio controlled aircraft with the maximum payload

possible. The aircraft presented in this paper, participated the 2009 competition under the acronym “UoP ATLAS” named after the Greek mythological titan Atlas.
The presentation of this work is an example where simple design principles, empiricisms, testing, and more sophisticated CFD and structural analysis methods, which are part of another paper, are used for the design and construction of a UAV, satisfying customer demands. The organization of this paper is as follows. In section II, the design requirements and the preliminary design based on them are given. In sections III-IV, the preliminary design, flight mechanics including the propulsion system are described. The preliminary design is based on linear aerodynamics and CFD analysis while flight mechanics analysis is performed on the preliminary design phase and is also based on linear analysis. In section V, aerodynamic analysis of the full UAV and optimization concepts base on CFD analysis are shown. Finally, in section VI conclusions and recommendations for further developments are presented.

2. PRELIMINARY DESIGN

Design limitations

The design of the aircraft had to satisfy the following restrictions: The maximum projected area not exceeding 0.70 m^2. The aircraft take off distance was limited to 60 meters of runway. The propulsion system was specified as a single AXI Gold 2820/10 (300W) motor and all the propulsion system and electronic parts had to fit in a transportation box 1100 x 500 x 400 mm. Extra bonus points for climbing with angle > 2^o was given. The aircraft had to take off and carry in flight a weight of 10 kg.

Weights estimation

Based on the above specifications the procedure followed for the calculation of the empty weight (W_E) differs from the traditional way of calculation which usually the literature[17-20] indicates due to the fact that the engine is given and the available power is known. Led by experience and taking into consideration data from similar aircrafts, a factor has been established which indicates that the aircraft takes off within a specified runway distance, empty weighted using the 30% of the available power of the engine. The above procedure gives an initial empty weight of 30.1N or approximately 3.0 kg. Given that the weight of the electronic equipment is approximately 0.78 kg, the remaining weight is distributed to the other components as shown in the Table 1. The weight is one of the limiting factors for the current design and the selection of the wing has to fulfil this design requirement.

Airfoil / Wing Calculations

The most critical value of the lift coefficient is considered the one corresponding to the take off phase. Due to ease of manufacturing, simplicity, and low cost considerations, we decided that there are no flaps, slats or any other lift enhancement device in our design. Therefore, the lift coefficient is also considered as the coefficient of lift for the flight phase. The required aerodynamic performance of the airfoil depends on the maximum takeoff weight (W_{TO}), which is designated by the goals of the team. Setting a range of the WTO between 8 and 14 kg and a takeoff speed VTO=15 m/s, the Eppler 420 airfoil was finally chosen. The range of the flight Reynolds number is 0.15 x 106 < Re < 0.55 x 106, where c is the wing mean chord length. The flow was considered as fully turbulent since the UAV normally flies in a high turbulent intensity environment. The airfoil, at this preliminary design phase was analyzed using the XFOIL code, and Navier-Stokes analysis. The results of Figures 1-4 show a comparison of the results using inviscid and viscous flow numerical solutions, obtained with FLUENT[21] and the Spalart-Allmaras[22] turbulence model. Taking into account, structural integrity and the design limitations, the wing aspect ratio is limited to 2.1m. A low wing configuration without flaps or slats is chosen, so that the aerodynamic performance is benefitted by the ground effect. There is no twist (ε_t) or dihedral (Γ_w) angle, and the angle of incidence of the wing was

set 60, where the L/D ratio is maximized according to the aerodynamic analysis of the airfoil. The characteristics of the initial wing design are shown in Table 2.

Component	Percentage of $W_{E_{initial}}$ (%)	Weight *(kg)*
Fuselage	14.4	0.442
Main wing	30	0.9204
Empennage	10	0.3068
Landing system	20	0.6136
Avionics	25.6	0.7852
Sum	100	3.068

Table 1 - Initial weight estimation and distribution

Wing Configuration	Low
Angle of sweep $\Lambda_{c/4}$	0°
Root airfoil thickness $(t/c)_r$	0.1429
Tip airfoil thickness $(t/c)_t$	0.1429
Taper ratio λ_w	0.43
Root chord length c_r (m)	0.39
Tip chord length c_t (m)	0.169245
Wing planform area S_w (m^2)	0.559245
Aspect Ratio AR	7.54

Table 2 - Wing characteristics

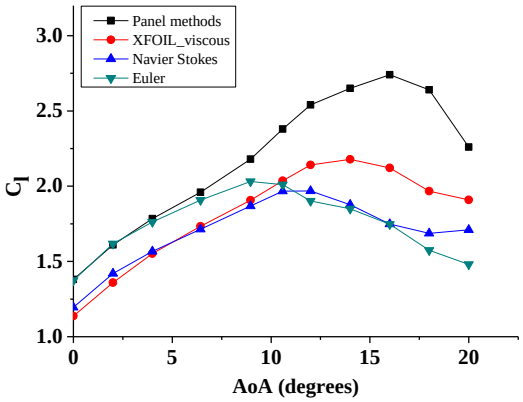

Figure 1 - Lift coefficient results after the airfoil analysis

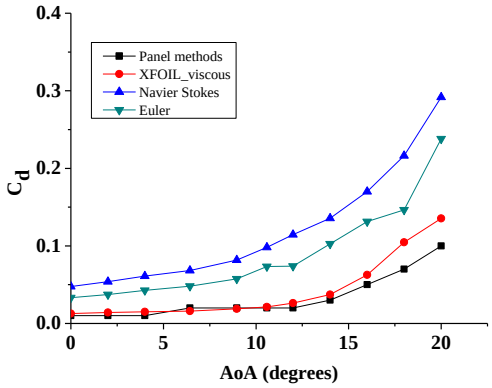

Figure 2 - Drag coefficient results after the airfoil analysis

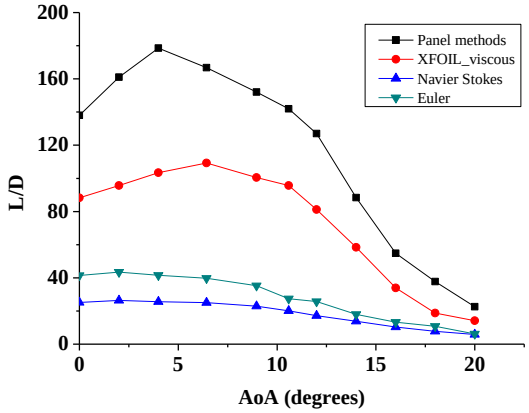

Figure 3 - L/D ratio results after the airfoil analysis

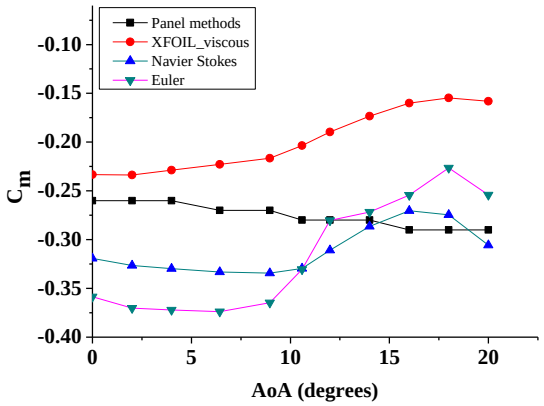

Figure 4 - Pitching moment coefficient results after the airfoil analysis

Fuselage Design

The process followed for the design of the cargo bay uses a bottom-up approach. Having the dimensions of the cargo bay, which are defined by the rules of the competition, the whole fuselage has been designed around it.
The main goals the design had to fulfill were the minimization of the "wetted area", the interference with the wing, the availability of many access points for loading / unloading and maintenance, and finally, strength to the applied aerodynamic and inertial loads. Three available options of the cross section shape, the circular, the rectangular and the double circle shape were evaluated according to the criterions of ease of manufacturing, performance and weight minimization. Finally, the rectangular cross section was chosen as shown in Figure 5. In the same figure is shown the arrangement of the equipment that yields a center of gravity approximately at the center of the cargo bay is shown.

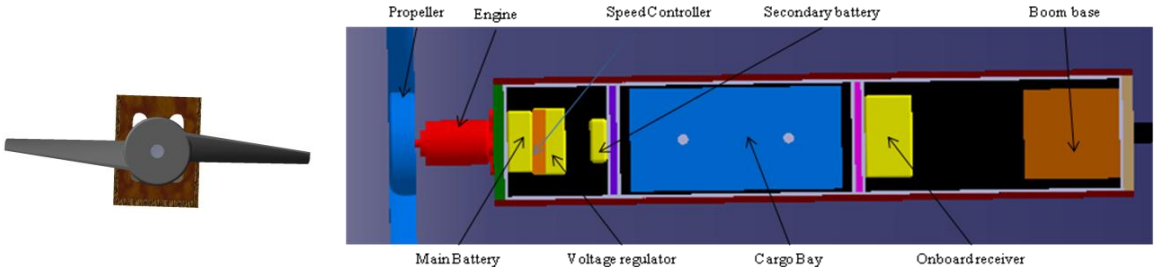

Figure 5 - Fuselage cross section and internal arrangement of the parts in the fuselage

Empennage initial design

Three possible configurations of the empennage were considered, a typical (inverted T-tail), a T-tail and a V-tail configuration. Finally, the typical configuration (see Fig.2) was selected. A carbon tube was used for the connection between the empennage and the fuselage because this option offers light weight and adjustability. For the horizontal and vertical stabilizers, NACA-0012 and NACA-0015 airfoil sections, respectively, were chosen. The initial dimensions of the stabilizers are summarized in Table 3.

	Horizontal Stabilizer	Vertical stabilizer
l_h	-5°	5°
(AR)	5	1.8
Λ	0°	1.5°
λ	1	0.4
c_{tip} (m)	0.162	0.12
c_{root} (m)	0.162	0.126

Table 3 - Initial dimensions of the empennage

Landing system design

Three possible configurations have been examined, the taildragger, the tricycle and the bicycle configuration. These configurations have been evaluated with criterions of ease of manufacturing, performance and weight. The tricycle configuration (see Figure 6) was chosen. Additional criterions are considered for the selection of the landing system, such as the position of the CoG and the ground clearance.

3. FLIGHT MECHANICS

Aerodynamic and flight mechanics analysis was performed on the design of Figure 6. Based on the aerodynamic loads, the empty weight and the 14 kg maximum take off weight load, structural analysis was performed. The presentation of these results is, however, outside of the scope of the present work.

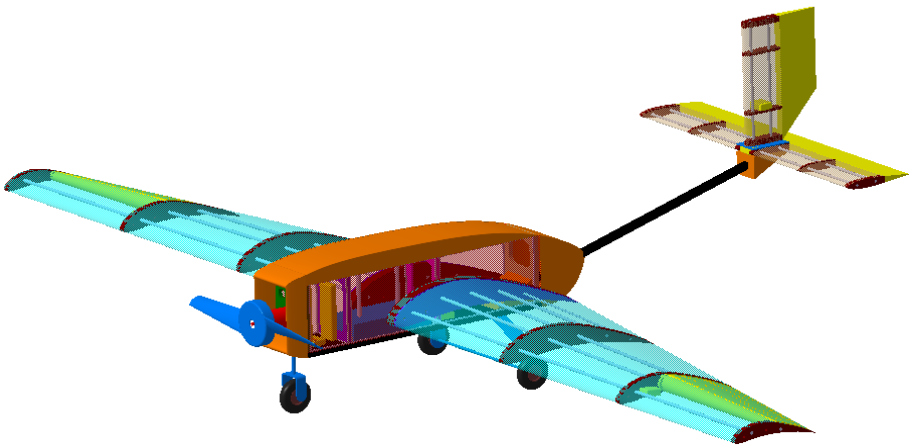

Figure 6 - ATLAS II preliminary design from CATIA

Flight mechanics analysis of the preliminary design yielded the drag coefficient and the required power during all phases of the flight envelope. Based on these the thrust of various propellers was estimated. Subsequently, the longitudinal, lateral, and yaw control analysis was performed and the final dimensions of the tail configuration and the control surfaces were extracted.

Calculation of the drag coefficient

The total drag coefficient has four main components: the wing drag, the fuselage drag, the empennage and the landing gear drag. The sum of these four components is multiplied by the constant factor 1.1 to include phenomena, such as the interference drag and the empennage induced drag. The wing drag component is, $C_{Dwing} = C_{Do,wing} + C_{Di,wing} = 0.11137$. The fuselage contributes only to the drag coefficient, as its lift is very small or zero, and its drag component is, $C_{Dfus} = 0.0012$. The empennage drag coefficient is the sum of the drag components of the horizontal and vertical stabilizers, $C_{Demp} = C_{D,ht} + C_{D,vt} = 0.01548$. For a non retractable landing gear system, the drag of the landing gear is considered $C_{Dgear} = 0.015$. The total drag is:

$$CD = 1.1\,(C_{Dwing} + C_{Dfus} + C_{Demp} + C_{Dgear}) = 0.14305 \quad (1)$$

The drag polar is obtained by the following relation[19-20] and is shown in Figure 7:

$$C_D = C_{D,o} + k\,C_L^2 = C_{Do,wing} + C_{Do,ht} + C_{Do,vt} + kC_L^2 = 0.01668 + kC_L^2 \quad (2)$$

Where, $k = 1 / \pi\, AR\, e = 0.047117$

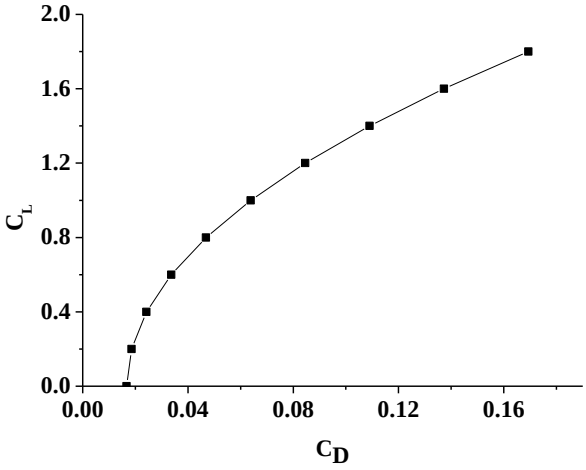

Figure 1 - Drag Polar

Propeller analysis

In order to determine to most efficient propeller for the aircraft, a number of propellers were tested with a custom built device. This experimental setup consists of an L-shaped arm, on one edge of the arm the engine was held and the other edge was connected on a digital scale. First, the scale was calibrated. Then the engine started and the measured force indication, F, on the scale was converted to static thrust via the formula: $T=F\ (L_F/L_T)$. Power (W) – Thrust (N), Electric Current (A) – Thrust (N), and Electric Current – Power (W) diagrams were extracted for each propeller measurement. These are shown in Figures 8-10. The cut off current is 40 A and, finally, three propellers appear to be as best choices: 11X4, 11X8 and 12X4 (diameter in cm x pitch) and the 12X4 propeller was selected.

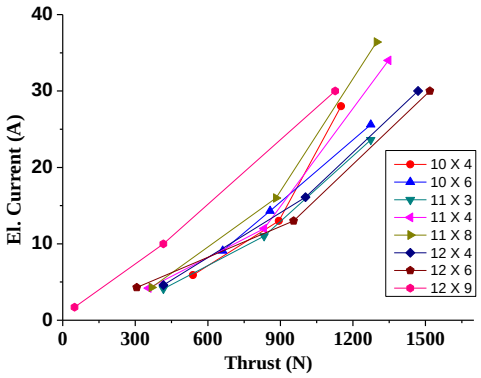

Figure 2 - El. Current (A) - Thrust (N) diagram

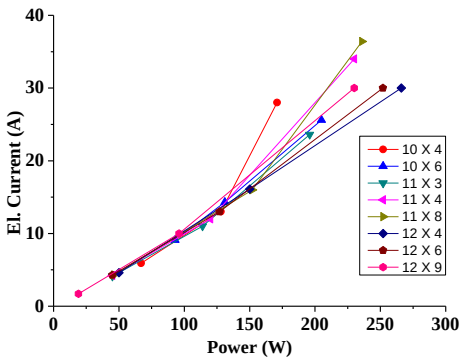

Figure 3 - El. Current (A) - Power (W) diagram

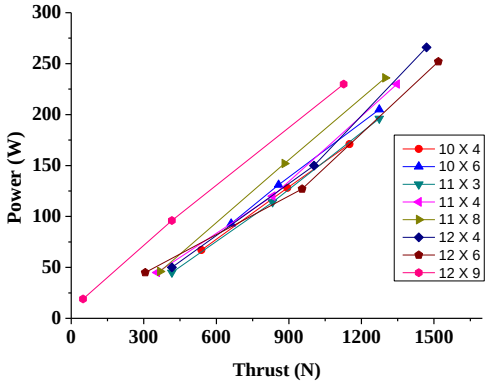

Figure4 - Power (W) - Thrust (N) diagram

Power Consumption

A simple flight profile including take-off, climb, loitering/maneuvering, decent, and landing was considered as representative of the of the mission profile of the aircraft. The power consumption during each of these phases is different, the sum of all these provides the total required power to complete the flight profile and thus the energy which the battery has to supply. Thus, equations-of-motion[19-20] for every phase of the flight profile were considered. The required thrust and power is calculated for each phase and are shown in Figures 11-19. The results showed that the most demanding phase is the climbing phase with a=2^{o} and, consequently, the W_{TO} is limited to 60N. The power consumption analysis is a critical stage of the entire design cycle. Currently this analysis was based on the specified electric motor. Clearly similar analysis should be performed when the electric motor should be replaced with an internal combustion engine.

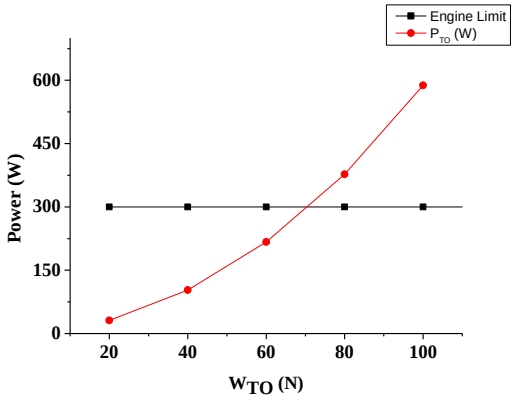

Figure 5 - Required power for take off

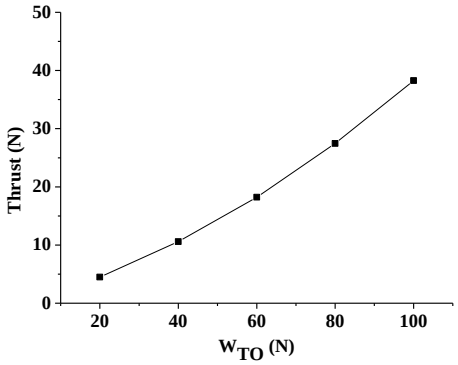

Figure 6 - Required thrust for take off

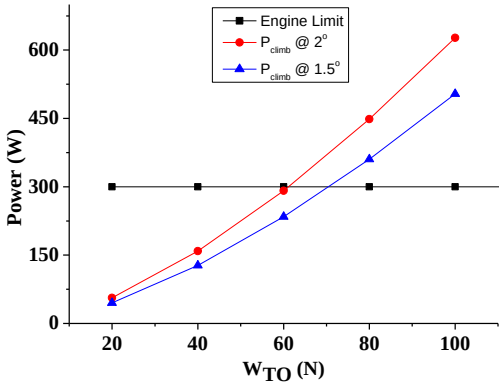

Figure 7 - Required power for 1.5° & 2° climbing

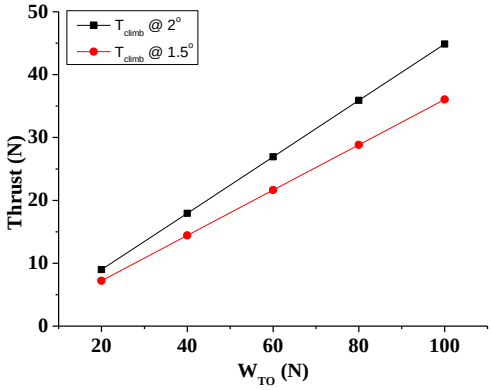

Figure 8 - Required thrust for 1.5° & 2° climbing

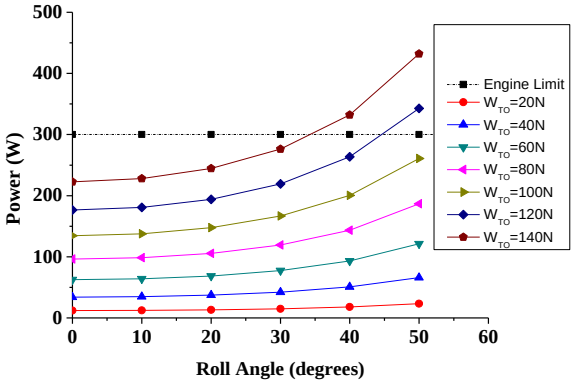

Figure 15 - Required power versus roll angle

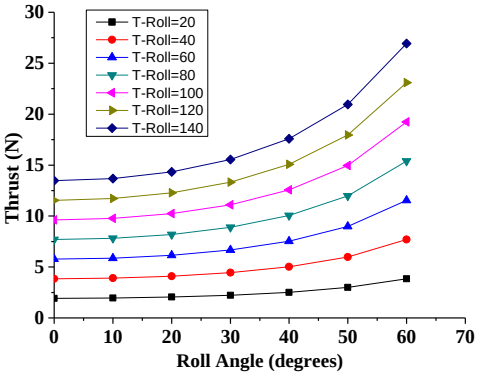

Figure 96 - Required thrust versus roll angle

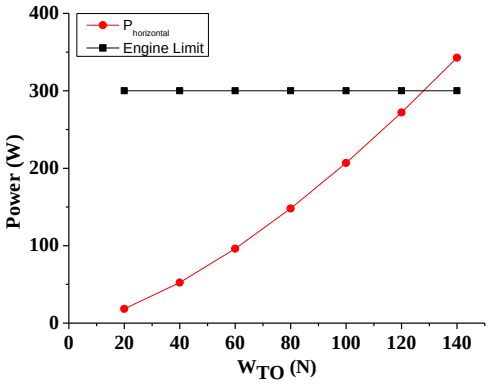

Figure 107 - Required power for level flight

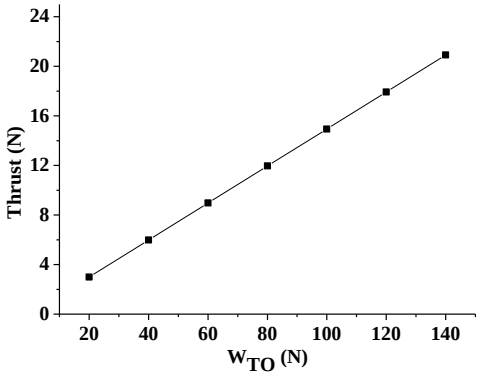

Figure 118 - Required thrust for level flight

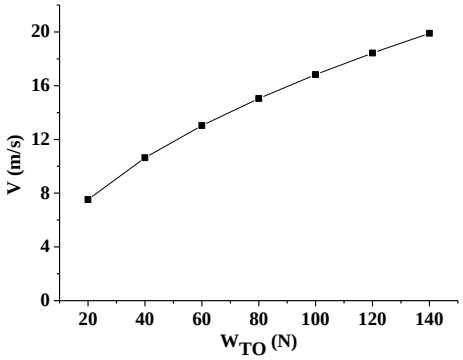

Figure 12 - Minimum rate of descent vs W_{TO}

Longitudinal control

The pitching moment around the center of gravity[19-20] is given by:

$$C_{m_{cg}} = C_{m_{0f}} + C_{m_{ac_w}} + \frac{dC_{m_f}}{d\alpha_f}\alpha_f + \frac{dC_{L_w}}{d\alpha}\alpha_w\left(\frac{h_{cg}}{\bar{c}} - \frac{h_{ac}}{\bar{c}}\right) - V_H n\left(\frac{dC_{L_t}}{d\alpha_t}\alpha_t + \frac{dC_{L_t}}{d\alpha_t}\tau\cdot\delta e\right) \quad (3)$$

The influence of the angle of attack of the horizontal stabilizer to the pitching moment coefficient is shown in Figure 20. The final dimensions of the horizontal stabilizer are presented in Table 4:

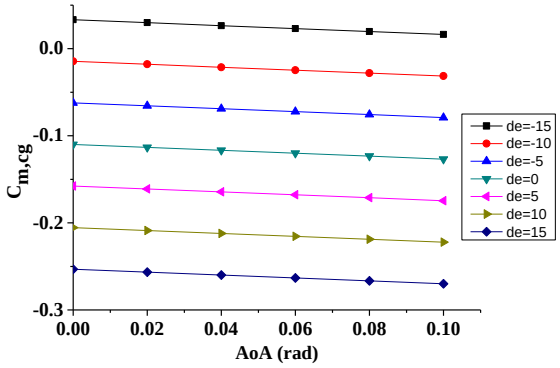

Figure 20 - Influence of the angle of attack of the horizontal stabilizer

Airfoil	NACA 0012
Planform area S_H *(m^2)*	0.0756
Aspect ratio AR_H	4.762
Span b_H *(m)*	0.6
Chord c_H *(m)*	0.126
Elevator planform area S_e *(m^2)*	0.03
Elevator span b_e *(m)*	0.6
Elevator chord c_e *(m)*	0.05

Table 4 - Final dimensions of the horizontal stabilizer

Lateral & Directional control

The ailerons are designed concurrently with the rudder, as they affect both directional and lateral control. The ailerons design is based on FAR 23, where an aircraft must be able to roll to 60 degrees of bank angle in less than 1.3 seconds. Structural considerations imposed the span to be proportional to the distance of the ribs of the wing (see Figure 6). The final dimensions of the ailerons are shown in Table 5.

For single engine UAVs, the critical condition for the vertical stabilizer design is the maximum crosswind landing. The final dimensions of the vertical stabilizer are shown in Table 6.

Planform area $\mathbf{S_A}$ **(m^2)** *(each)*	0.0337
Aspect ratio $\mathbf{AR_A}$	2.4
Span $\mathbf{b_A}$ **(m)**	0.32
Root chord $\mathbf{c_{rA}}$ **(m)**	0,14065
Tip chord $\mathbf{c_{tA}}$ **(m)**	0.07
Mean chord $\mathbf{c_{mA}}$ **(m)**	0.10532
$\mathbf{S_A / S_W}$	0.12

Table 5 - Final dimensions of the ailerons (each)

Airfoil	NACA 0015
Planform area S_V *(m^2)*	0.0375
Aspect ratio AR_V	2.4
Span b_V *(m)*	0.3
Chord c_V *(m)*	0.125
Rudder planform area S_r *(m^2)*	0.01125
Rudder span b_r *(m)*	0.2
Rudder chord c_r *(m)*	0.05625

Table 3 - Final dimensions of the vertical stabilizer

4. AERODYNAMIC ANALYSIS AND OPTIMIZATION

Evaluation and possible modifications for optimization of the UAV design of Figure 2 that was performed based on linear aerodynamic analysis, as outlined in the previous sections, could be achieved with wind tunnel testing. However one constraint for UAV's, including the present design, is low cost. In the preliminary phase it has been already mentioned that several compromises were made in terms of shape, for example a rectangular cross section was selected, in order to minimize manufacturing cost. Wind tunnel testing, even for the maximum flight Reynolds number ($Re_c \approx 0.5 \times 10^6$) of the present configuration at maximum flight speed $U_\infty \approx 20$m/sec is possible but prohibitively expensive. Therefore evaluation of the full scale aerodynamics of the present design that was eventually successfully fulfilled the requirements of the competition, was performed with CFD analysis.

The CATIA[23] exported STEP file of the design was used to extract the geometry and construct unstructured hybrid type meshes. Meshes for surfaces, components (wing/fuselage), and complete configurations were constructed using the ANSA V13 pre-processor.[24] Starting from the CATIA exported geometry complete meshes for viscous and inviscid flow calculations were completed in less that one day.

The computational mesh for the full configuration where the surface discretization is shown is presented in Figure 21. The entire UAV surface was discretized with 60,000 triangular elements with a variable size triangular surface mesh. Mapped meshes were used only for the aerodynamic surfaces in order to keep the mesh count low while maintaining a close representation of the curvature and achieve concentration of cells at areas of interest. The model is placed in a large (50mx20mx15m) exterior domain. Only a half symmetric model is created. From the triangular elements of the surface a layer of 30 prismatic (pentahedral) elements was constructed for accurate capturing of the near wall flow. The height of the first element was sufficiently small to ensure accurate computation of the turbulent flow at the flight Reynolds number. The growth factor of the near wall elements was less than 1.2 to ensure that the near wall flow is captured with sufficient number of cells. The space between the ends of the prismatic layers to the far field was filled with tetrahedral elements. The ANSA grid generation software[24] provides the flexibility of specifying a maximum element length in a box (size box) where elements are constructed. Size boxes (see Figure 21) are used around the airplane, its wake, and the trailing vortex path in order to keep the cell size low enough in these regions. The area of increased resolution is clearly visible in Figure 21. The mesh for the complete UAV contains 8.1×10^6 elements and 2.8×10^6 nodes. Numerical solutions were computed with commercial CFD software ANSYS FLUENT v6[21]. The field mesh contains the propeller plane as a circular disk that could be used with the actuator disk model of FLUENT. However, in our computations this feature was not activated.

Two wing shapes were considered a baseline wing as in the original design and a wing with tip fence and smooth blending with the fuselage. The detail of the mesh around these wings is shown in Figures 22 and 23. Performance enhancements (higher lift and lower drag) were obtained with the addition of the smooth wing fuselage blending and the tip fence. Therefore this configuration was used for the final design. A mesh that was constructed for the evaluation of ground effect is shown in Figure 24. The same surface discretization was used and a mesh was constructed for the wing fuselage configuration only in order to investigate the effect of ground during take off and landing. This mesh was deformed using an automatic feature of the ANSA[24] grid generation package in order to obtain configurations at different incidences. A sample deformed mesh at incidence angle a=6 deg. is shown in Figure 24.

In the lack of wind tunnel testing, we used CFD analysis to test aerodynamic enhancement concepts at a relatively low cost. Considering that a steady-state numerical solution for each angle of incidence could be obtained in few hours CFD analysis is a viable means of testing. For example, a converged solution in four processors is obtained in six hours of CPU time. Therefore a complete load curve is obtained in two days and this time is diminished with the increase of the number of processors. In most simulations, it was assumed that the flow is fully turbulent and the Spalart-Allmaras[22] turbulence model was used. For the baseline case (horizontal flight at incidence α=0 deg.) the flow was computed with the $k - \omega$ SST turbulence model and for transitional flow modeling with the $k - \omega$ SST model.[25, 26] Small differences of the computed surface flow and for the overall loads were obtained for computations with difference turbulence models and with transition. The differences of the surface flow over the wing are illustrated in Figure 25. It appears that the $k - \omega$ SST turbulence model predicts more separation at the trailing edge region. However, the differences in surface flow for the computation with transitions are very small perhaps due to the large value of the free stream truculence intensity that was specified.

The computed loads for a range of angles of incidence are shown in Figures 26 and 27. Clearly, the improved design with a fence and smooth wing fuselage blending yields higher lift and it was selected for the UAV. The lift is sufficient for the flight of the UAV with the specified load. Furthermore, the computed pitching moment of Figure 27 demonstrates that the UAV designs with and without tips are both stable in longitudinal flight. The value of

total drag that was obtained with the transitional flow computation is the lowest. The lift values at α = 0 deg. computed with the *k* – *ω* SST are lower than values obtained with the SA model as the surface flow of Figure 25 indicates.

The effect of ground is shown in Figure 28. It appears that significant ground effect is obtained. Additional CFD analysis for other airfoil shapes, mounting of the wing on the fuselage, and use of lift enhancement devices, such as flaps could be used to obtain improvements of the current design that is shown in draft in Figure 29 and in flight in Figure 30.

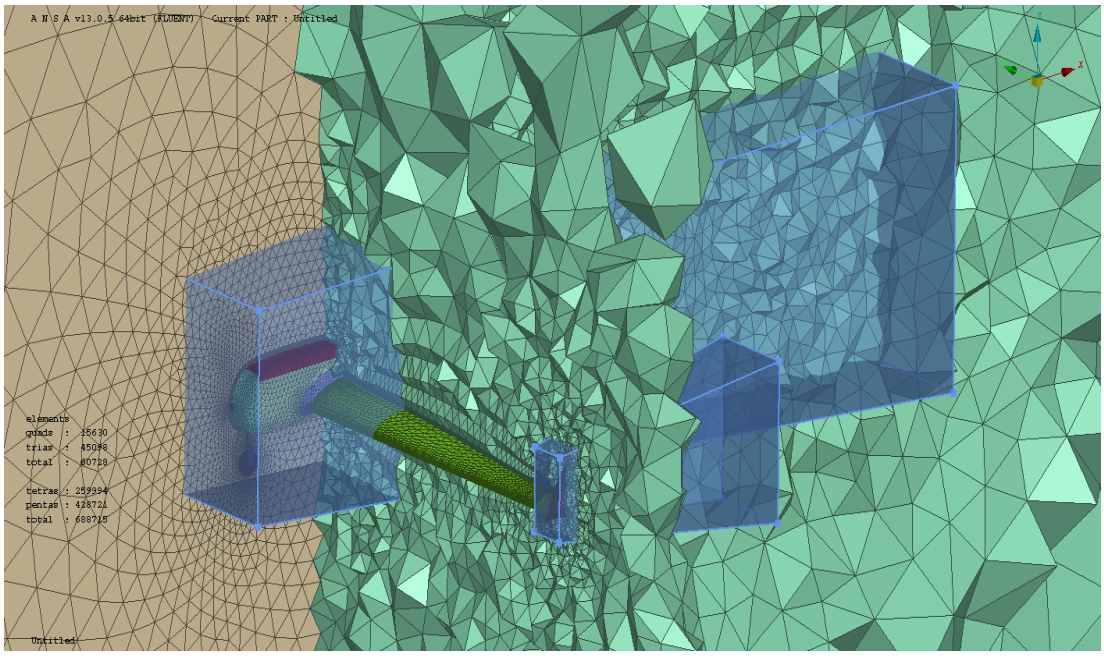

Figure 13 - Overall view of the mesh with the boxes where refined mesh is enforced

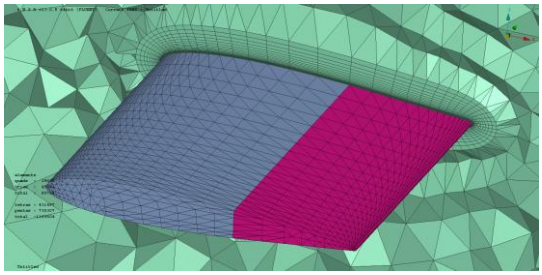

Figure 14 - Rear wing designs

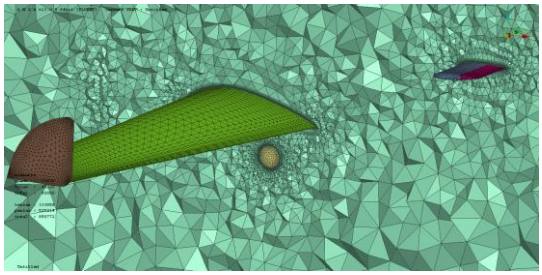

Figure 15 - Wing designs with tip fence

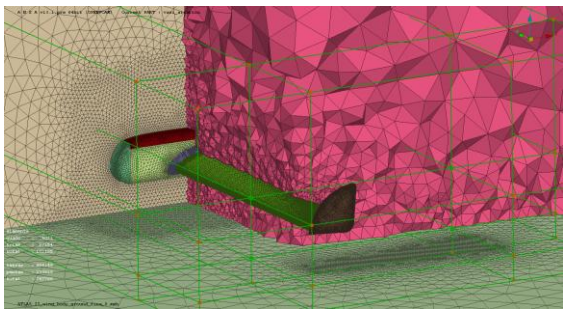

(baseline α = 0 deg)

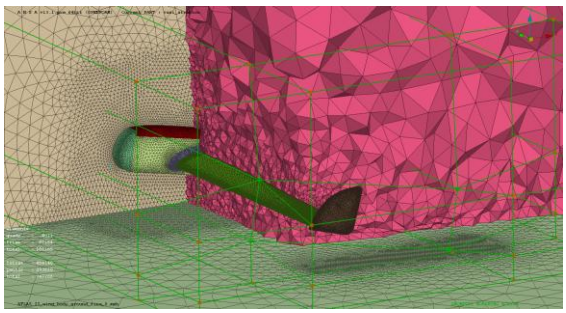

(deformed α = 6 deg)

Figure 16 Fuselage wing at incidence α = 0 deg and deformed mesh at α = 6 deg.

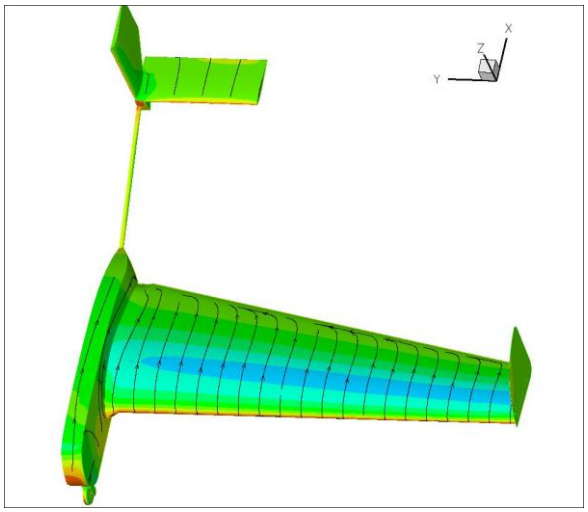

SA

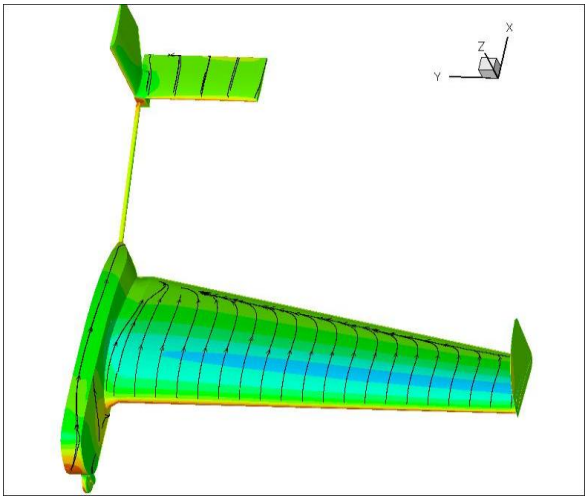

k-ω-SST

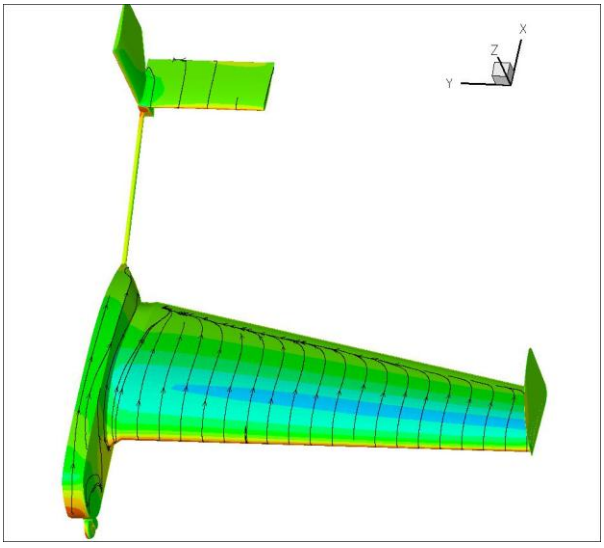

k-ω-SST transition

Figure 25 Surface flow on the wing for computations performed with (a) the S-A model (b) the *k – ω* SST turbulence model, and (c) *k – ω* SST turbulence model with transition at a=0^{o}

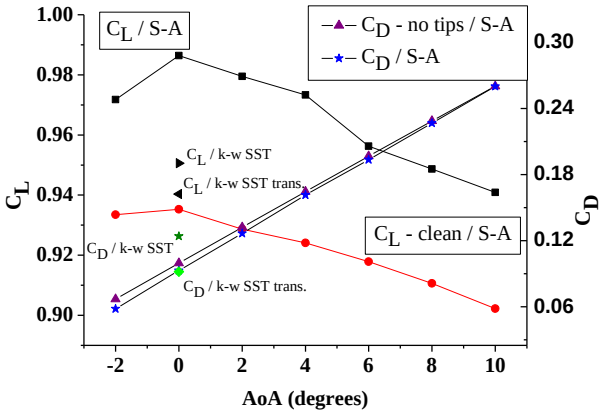

Figure 26 - Computed lift and drag for tips and no tips wing configurations.

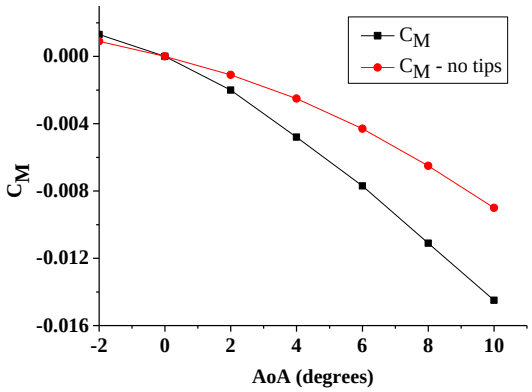

Figure 27 - Computed pitching moment for tips and no tips wing configurations.

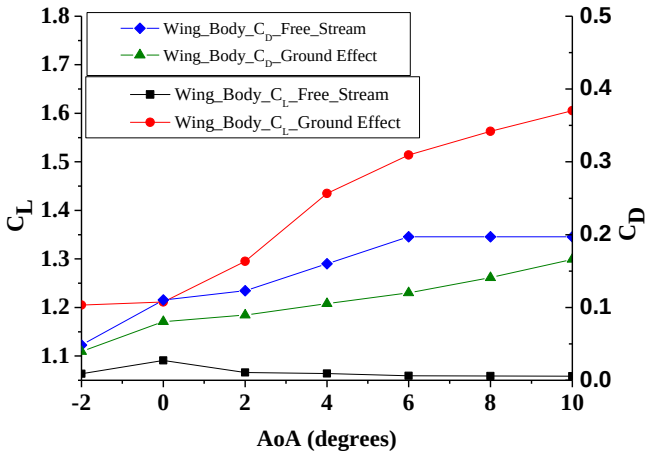

Figure 28 - Effect of ground proximity on the computed lift and drag.

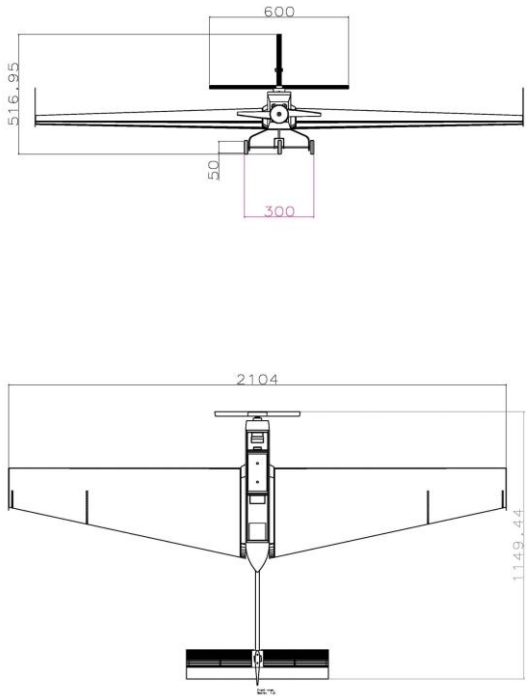

Figure 29 - Draft and dimensions, final design.

Figure 30 - Atlas take off and flight

5. CONCLUSIONS

A light cargo UAV was designed, build, and successfully tested in flight. The design fulfilled criteria set in a student competition. A preliminary design was obtained using linear analysis. Linear flight mechanics analysis was used to achieve controlled stable flight. The propulsion system was carefully selected using in-house propeller testing. Aerodynamics enhancements were achieved using CFD analysis for the full configuration. Additional numerical tests demonstrated that sufficient ground effect could be obtained to facilitate the takeoff phase. The proposed UAV design was successfully tested in flight and it could be further enhanced using CFD analysis.

REFERENCES

(1) Bradley, T. H., Moffitt, B. A., Fuller, T. F., Mavris, D. N., and, Parekh, D. E., “Comparison of Design Methods for Fuel-Cell-Powered Unmanned Aerial Vehicles” Journal of Aircraft, Vol. 46, No. 6, 2009, pp. 1945 – 1956.

(2) Stone, R. H., “ Aerodynamic Modeling of the Wing-Propeller Interaction for a Tail-Sitter Unmanned Air Vehicle", Journal of Aircraft, Vol. 45, No. 1, 2008, pp. 198 – 209

(3) Dufresne, S., Johnson, C., and Mavris, D. N., “Variable Fidelity Conceptual Design Environment for Revolutionary Unmanned Aerial Vehicles,” Journal of Aircraft, Vol. 45, No. 4, 2008, pp. 1405 – 1418.

(4) Sadraey, M. and Colgren R. “A Systems Engineering Approach to the Design of Control Surfaces for UAVs,” AIAA Paper 2007-660 45th ASM, Reno, NV, 8 – 11 Jan. 2007.

(5) Hsiao F. B., Chan, W. L., Lai, Y. C., Tseng, L. C., , Hsieh, S. Y.,, and Tenn, H. K., “Landing Longitudinal Control System Design for a Fixed Wing UAV,” AIAA Paper 2007-868, 45th AIAA ASM, Reno NV, 8 - 11 Jan. 2007.

(6) Harmon, F. G., Frank, A. A., and Chattot, J. J., “Conceptual Design and Simulation of a Small Hybrid-Electric Unmanned Aerial Vehicle,” . of Aircraft, Vol. 43, No. 5, 2006, pp. 1490 – 1498.

(7) Nagel, A., Levy, D. E., and Shepshelovich, M., “Conceptual Aerodynamic Evaluation of MINI/MICRO UAV,” AIAA Paper 2006-1261, 44th AIAA ASM, Reno NV, 9 - 12 Jan. 2006.

(8) Nagel, A and Shepshelovich, M., “Development of High-Lift UAV Wings,” AIAA Papre 2006-3467, 24th Applied Aerodynamics Conference,, San Francisco, CA, 5 - 8 June 2006.

(9) Dogan, A. and Venkataramanan, S., “Modeling of Aerodynamic Coupling Between Aircraft in Close Proximity”, Journal of Aircraft, Vol. 42, No. 4, 2005, pp. 941 – 955.

(10) D. Lorenz, R. D., “Flight Power Scaling of Airplanes, Airships, and Helicopters: Application to Planetary Exploration” Journal of Aircraft, Vol. 38, No. 2, 2001, pp. 208 – 214.

(11) Gur, O., Mason, W. H. And J. A. Schetz, “Full Configuration Drag Estimation”, AIAA Paper 2009-4109, 27th Applied Aerodynamics Conference, 22-25 June 2009, San Antonio, TX.

(12) Prudente, D. M. and A. V. G. Cavalieri, “Tail and Control Surface Sizing for UAVs, AIAA 2007-4557, 25th Applied Aerodynamics Conference, 25-28 June 2007, Miami, FL, USA.

(13) Wick, A. T., Zink, G. A., Ruszkowski, R. A. Jr, and Shih, T. I. P., “Computational Simulation of an Unmanned Air Vehicle Impacting Water,” AIAA Paper 2007-70, , Reno NV, 8 - 11 Jan. 2007.

(14) Moyer, S. A. and Talbot, M. D., “Wind-Tunnel Test Techniques for Unmanned Aerial Vehicle Separation Investigations,” Journal of Aircraft, Vol. 31, No. 3, 1994, pp. 585 – 590.

(15) Shafer, T. C., and Green, B. E., “CFD Generation of Flight Databases for UAVs for Use in the Flight Certification Air-Worthiness Process,” AIAA Paper 2010-1037, 4 - 7 Jan. 2010.

(16) Kim, C., and Lee, J. Y, "Numerical Analysis of Hovering Tilt-Rotor UAV for Minimum Download and Ground Effect Analysis," AIAA Paper 2007-1400, Reno, NV, 8 - 11 Jan. 2007.
(17) Anderson, J.A. Jr., "Fundamentals of Aerodynamics", 3rd Edition, Mc Graw Hill, New York, USA, 2001.
(18) Simons, M., "Model Aircraft Aerodynamics", Argus Books, England, 1994.
(19) Roskam, Jan, "Airplane Design", Roskam Aviation & Eng. Corporation, Kansas, USA, 1985.
(20) Roskam, Jam and Chuan-Tau Edward Lan, "Airplane Aerodynamics & Performance", DAR Corporation, Kansas, USA, 1997.
(21) Fluent Inc., FLUENT 6.3 User's Guide, USA, 2006. Spalart, P. and S., Allmaras, "A One-Equation Turbulence Model for Aerodynamic Flows", American institute of Aeronautics and Astronautics (AIAA), AIAA Paper 92-0439.
(22) Spalart, P. and S., Allmaras, "A One-Equation Turbulence Model for Aerodynamic Flows", AIAA Paper 92-0439, Jan. 1992.
(23) Dassault Systemes, CATIA V5 User Manual, France, 2007.
(24) ANSA version 13.0.2 User's Guide, BETA CAE Systems S.A., September 2009
(25) Menter, F. R.,Langtry, R., and Völker, S., "Transition Modelling for General Purpose CFD Codes," Flow Turbulence and Combustion, 2006, Vol. 77, 2006, pp. 277–303.
(26) Langtry, R. and Menter, F. R., "Transition Modeling for General CFD Applications in Aeronautics" AIAA Paper 2005-522, Reno NV, Jan. 2005.